

GENERAL ARTICLE

Aberrant lung lipids cause respiratory impairment in a *Mecp2*-deficient mouse model of Rett syndrome

Neeti Vashi^{1,2}, Cameron Ackerley³, Martin Post³ and Monica J. Justice^{1,2,*}

¹Department of Molecular Genetics, University of Toronto, Toronto, Ontario M5S 1A1, Canada, ²Genetics and Genome Biology Program, Hospital for Sick Children, Peter Gilgan Centre for Research and Learning, Toronto, Ontario M5G 0A4, Canada and ³Translational Medicine Program, Hospital for Sick Children, Peter Gilgan Centre for Research and Learning, Toronto, Ontario M5G 0A4, Canada

*To whom correspondence should be addressed at: 686 Bay Street, Toronto, Ontario M5G 0A4, Canada. Email: monica.justice@sickkids.ca

Abstract

Severe respiratory impairment is a prominent feature of Rett syndrome, an X-linked disorder caused by mutations in methyl CpG-binding protein 2 (*MECP2*). Despite *MECP2*'s ubiquitous expression, respiratory anomalies are attributed to neuronal dysfunction. Here, we show that neutral lipids accumulate in mouse *Mecp2*-mutant lungs, whereas surfactant phospholipids decrease. Conditional deletion of *Mecp2* from lipid-producing alveolar epithelial 2 (AE2) cells causes aberrant lung lipids and respiratory symptoms, whereas deletion of *Mecp2* from hindbrain neurons results in distinct respiratory abnormalities. Single-cell RNA sequencing of AE2 cells suggests lipid production and storage increase at the expense of phospholipid synthesis. Lipid production enzymes are confirmed as direct targets of *MECP2*-directed nuclear receptor co-repressor 1/2 transcriptional repression. Remarkably, lipid-lowering fluvastatin improves respiratory anomalies in *Mecp2*-mutant mice. These data implicate autonomous pulmonary loss of *MECP2* in respiratory symptoms for the first time and have immediate impacts on patient care.

Introduction

Altered pulmonary lipid metabolism is a feature of many respiratory diseases. Pulmonary surfactant, a lipid-rich complex of phospholipids, proteins and neutral lipids, is essential for lowering surface tension in the lung and preventing alveolar collapse (1). The abundance and species composition of surfactant lipids requires tight control; phosphatidylcholines (PCs) represent 85% of the lipids in pulmonary surfactant, whereas phosphatidylglycerols make up 11%. Other components, including cholesterol and other neutral lipids are present, though the

role of triglycerides (TGs) in the lung has not been well defined (2).

Pulmonary surfactant is an absolute requirement for normal gas exchange. Preterm infants born before producing enough surfactant develop respiratory distress syndrome (3). Mutations in surfactant production genes, surfactant-protein B (*SFTPB*), C (*SFTPC*), or the lipid transporter ATP-binding cassette subfamily A member 3 (*ABCA3*) cause surfactant dysfunction; neonates born with these mutations generally experience respiratory failure due to low quantities of surfactant phospholipids and surfactant dysfunction (4–6). In addition, reduced activity of sterol

Received: March 26, 2021. Revised: May 11, 2021. Accepted: June 28, 2021

© The Author(s) 2021. Published by Oxford University Press. All rights reserved. For Permissions, please email: journals.permissions@oup.com

This is an Open Access article distributed under the terms of the Creative Commons Attribution Non-Commercial License (<http://creativecommons.org/licenses/by-nc/4.0/>), which permits non-commercial re-use, distribution, and reproduction in any medium, provided the original work is properly cited.

For commercial re-use, please contact journals.permissions@oup.com

regulatory element-binding protein (SREBP), a lipid-sensing transcriptional activator, increases lung cholesterol and TGs while decreasing phospholipids in mice (7).

Breathing abnormalities, including hyperventilation, apneas and breath holds, are a prominent feature of Rett syndrome (RTT), a severe neurological condition (8). RTT is caused by mutations in the X-linked gene methyl CpG-binding protein 2 (MECP2) (9). Affected patients reach normal developmental milestones until 6–18 months of age, when they experience a developmental regression involving loss of acquired verbal and motor skills, stereotypic hand wringing and seizures (10). Respiratory dysfunction causes up to 80% of RTT patient deaths (11), but has been historically attributed to autonomic disturbances and brainstem dysfunction, as RTT has been predominately described as a neurological disease (12–14). *Mecp2*-mutant mice display similar respiratory disturbances as patients including altered breathing frequency and increased apneas (15). Although female *Mecp2*^{+/+} mice are more clinically relevant, male *Mecp2*^Y mice are generally studied for their early symptom onset and consistent phenotype. To date, treatments aimed at dampening the hyperexcitation of brainstem nuclei or modulating neurotransmission through targeting the brain derived neurotrophic factor (BDNF), gamma aminobutyric acid (GABA), dopamine and serotonin systems in the respiratory neural network in *Mecp2*-mutant mice have modestly or transiently improved breathing (16–22), implying other factors are involved in respiratory symptoms.

MECP2 is a ubiquitously expressed transcriptional regulator whose primary role is to bridge methylated DNA with the nuclear receptor co-repressor 1/2 (NCOR1/2) complex (23,24). The interaction between MECP2 and the NCOR1/2 complex is facilitated by MECP2's amino acids 298–309, which bind to complex members transducin beta-like 1 X-linked (TBL1X) and TBL1X receptor 1 (TBL1XR1) (23,25,26). When *Mecp2* is mutated, this complex binds to chromatin with a lower efficiency, resulting in the loss of repression of numerous genes (27). NCOR1, with complex member histone deacetylase 3 (HDAC3), regulates lipid metabolism (28,29); our laboratory has shown that loss of *Mecp2* diminishes the recruitment of the NCOR1/2 complex to the promoters of lipogenic enzymes in the mouse liver, resulting in hepatic steatosis (30).

MECP2 is highly expressed in the mouse and human lung (31,32). Despite this, the lung is greatly understudied in the RTT field. As the lung represents a major site of *de novo* lipogenesis, lung lipid metabolism genes may be a target of MECP2-directed transcriptional regulation. Here, we report that *Mecp2* deletion drastically alters lung lipid composition due to decreased binding of the NCOR1/2 co-repressor complex at lipid metabolism genes. These findings challenge the view that RTT symptoms result solely from loss of neuronal MECP2, inform on MECP2's role as a transcriptional regulator in non-neuronal tissue and point to new therapeutic strategies for RTT.

Results

Mecp2 deletion results in abnormal lipid production in the mouse lung

To visualize changes in lung structure that could contribute to breathing symptoms in *Mecp2*^Y mice, transmission electron microscopy (TEM) was performed on perfused, inflation-fixed lungs. Lipid accumulation was present in postnatal day (P) 56 *Mecp2*^Y mouse lungs, a time point after the onset of symptoms (symptomatic) (Fig. 1A). Lipid droplets were confirmed by

histological staining (Fig. 1B, Supplementary Material, Fig. S1A and B) and were absent in age-matched +/Y mice. Although brain and liver lipid metabolism defects are present in *Mecp2*-mutant mice (30,33), the observation of aberrant lung lipids was unexpected. Female *Mecp2*^{+/+} mice, a more clinically relevant model, also exhibit drastic lung lipid accumulation at the peri- and post-symptomatic time points of 6 and 9 months of age, respectively, with a more dramatic progression likely due to their longer lifespan (Fig. 1C and D).

High-performance liquid chromatography (HPLC) was used to quantify lung lipids. In the lung, *de novo* lipid synthesis produces pulmonary surfactant, a biochemically heterogeneous complex of lipids and proteins that lines the epithelial layer to facilitate normal gas exchange. Consistent with the TEM findings, *Mecp2*^Y mice have excess TGs in their lungs at the pre-symptomatic time point of P21 (5.31 ± 0.56 mg/g in +/Y; 9.46 ± 0.58 in *Mecp2*^Y, $P = 0.002$) and the symptomatic time point of P56 (11.15 ± 1.18 mg/g in +/Y; 19.39 ± 2.15 in *Mecp2*^Y, $P = 0.015$) (Fig. 1E). *Mecp2*^Y mice also have excess cholesterol in their lungs at P21 (2.39 ± 0.19 in +/Y; 3.00 ± 0.06 in *Mecp2*^Y, $P = 0.022$) but not at P56 (Fig. 1F). Therefore, lung lipid accumulation precedes respiratory and behavioral symptoms, which typically appear at ~P28.

To quantify lipids in the pulmonary surfactant, bronchoalveolar lavage (BAL) fluid was subjected to liquid chromatography-mass spectrometry (LC-MS/MS). Dipalmitoylphosphatidylcholine (DPPC) is the major constituent of pulmonary surfactant, making up ~40% of its normal composition. DPPC is the strongest surface-active molecule in the pulmonary surfactant mixture. Other PC molecules in lung surfactant regulate its fluidity. DPPC was markedly reduced in the *Mecp2*^Y BAL fluid at both P21 (156.91 ± 12.58 µg/ml in +/Y; 64.80 ± 3.02 in *Mecp2*^Y, $P = 0.0024$) and P56 (117.58 ± 3.96 µg/ml in +/Y; 86.78 ± 9.38 in *Mecp2*^Y, $P = 0.0116$) (Fig. 1G). Other PC species were also detected at lower quantities in *Mecp2*^Y BAL fluid (Supplementary Material, Fig. S1D and F), but total lung PCs were not changed (Supplementary Material, Fig. S1C and E). Finally, cholesterol was increased in *Mecp2*^Y BAL at P21 (2431.25 ± 283.52 µg/ml in +/Y; 3643.25 ± 381.76 in *Mecp2*^Y, $P = 0.0436$), but was at normal levels by P56 (Fig. 1H). Altogether, these findings indicate an increase in cholesterol and neutral lipids in the lung tissue with a parallel decrease in PCs in the BAL fluid.

Female *Mecp2*^{+/+} mice also have elevated lung TGs at 3 months of age (6.87 ± 0.35 mg/g in +/+; 8.80 ± 0.41 in *Mecp2*^{+/+}, $P = 0.012$), and this elevation remains over the course of disease progression up to 12 months ($P < 0.05$, Fig. 1I). In contrast, lung cholesterol transiently increases at 6 months in *Mecp2*^{+/+} lungs, during the peri-symptomatic period (4.48 ± 0.47 mg/g in +/+; 6.38 ± 0.25 in *Mecp2*^{+/+}, $P = 0.012$) (Fig. 1J). DPPC (PC 32/0) was markedly decreased in *Mecp2*^{+/+} BAL fluid at both 6 months (117.58 ± 7.9 µg/ml in +/+; 88.14 ± 3.8 in *Mecp2*^{+/+}, $P = 0.016$) and 9 months of age (115.02 ± 3.25 µg/ml in +/+; 85.09 ± 11.9 in *Mecp2*^{+/+}, $P = 0.045$) (Fig. 1K), and again, other PC species were altered (Supplementary Material, Fig. S1G–H). However, BAL cholesterol was unchanged at both time points (Fig. 1L).

Conditional deletion of *Mecp2* from mouse lung is sufficient to cause lung lipid accumulation and respiratory symptoms

In the lung, alveolar epithelial 2 (AE2) cells are metabolically and functionally complex epithelial cells whose primary role is to synthesize, secrete and recycle pulmonary surfactant. AE2 cells produce all subclasses of surfactant lipids, including PCs and

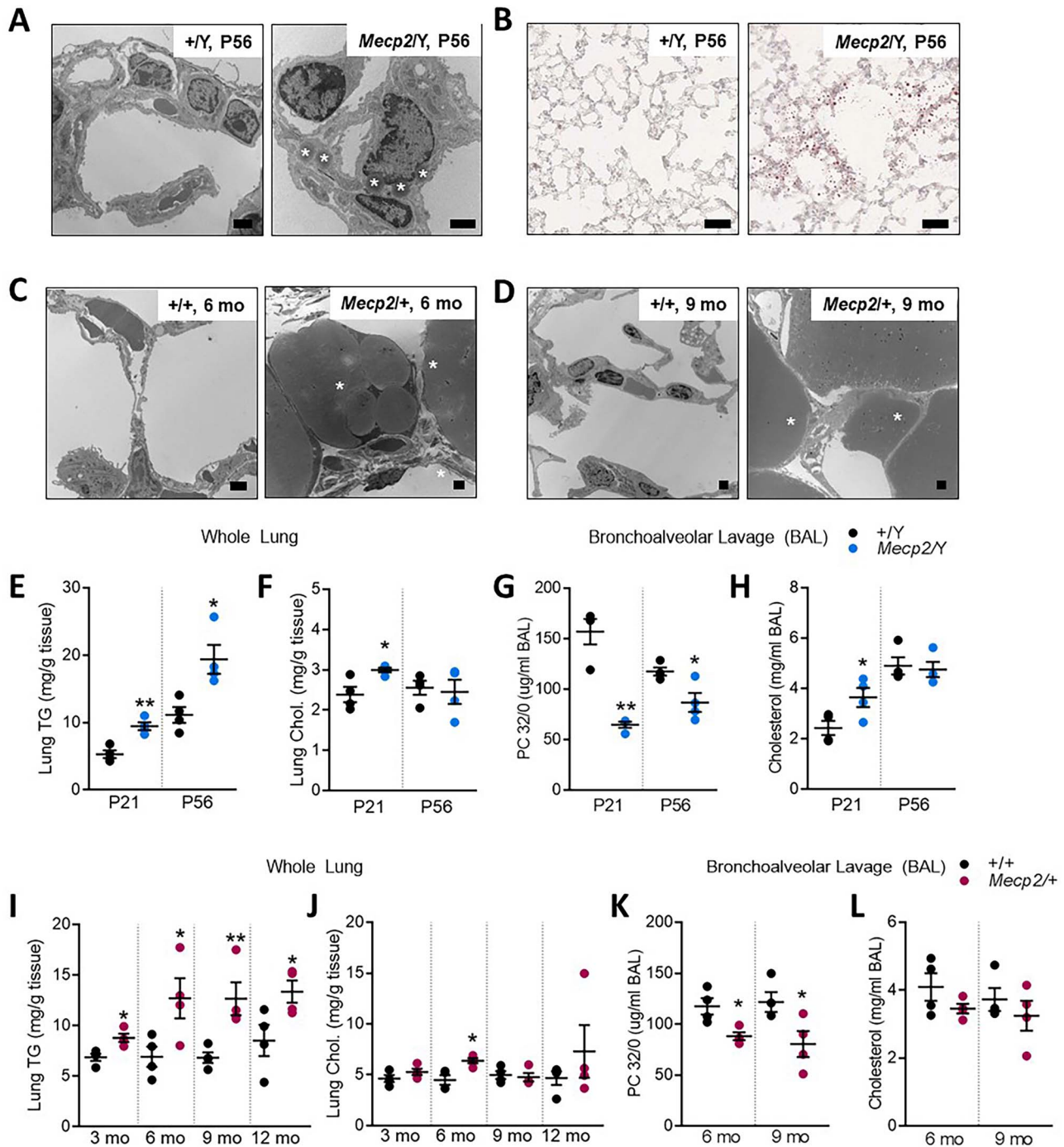


Figure 1. *Mecp2* deletion alters lipid composition of the mouse lung. (A) Electron micrographs of the alveolar area of the lung in male *+/Y* and *Mecp2/Y* mice at P56. Scale bars represent 2 μ m. Asterisk indicates lipid droplets. (B) Oil Red O staining of neutral lipids (red) in alveoli of male *+/Y* and *Mecp2/Y* mice at P56. Scale bars represent 50 μ m. Electron micrographs of female *+/+* and *Mecp2/+* lungs at (C) 6 months and (D) 9 months. Scale bars represent 2 μ m. Asterisk indicates lipid droplets, $n = 2$ per age/genotype. Whole-lung (E) triglycerides and (F) cholesterol as measured by high-performance liquid chromatography in *+/Y* and *Mecp2/Y* mice, $n = 4$. Bronchoalveolar lavage (BAL) fluid (G) PC 32/0 (dipalmitoylphosphatidylcholine, DPPC) and (H) cholesterol as measured by LC-MS/MS in *+/Y* and *Mecp2/Y* mice, $n = 4$. Lung (I) triglycerides and (J) cholesterol and BAL fluid (K) PC 32/0 and (L) cholesterol in female *+/+* and *Mecp2/+* mice, $n = 4$. Data are expressed as mean \pm SEM. Statistics were performed using Student's *t*-test. * $P < 0.05$, ** $P < 0.01$.

neutral lipids. *Mecp2*^{tm3.1Bird} mice, which have a green fluorescent protein (GFP) tag fused to the endogenous *Mecp2* locus, were used to visualize expression. High MECP2 expression was present in lung AE2 cells (Fig. 2A), consistent with previous reports in mouse and human (32,34).

Therefore, *Mecp2* deficiency in lung AE2 cells alone could alter lung lipid metabolism, which may contribute to abnormal breathing in *Mecp2*-mutant mice. As respiratory symptoms of RTT are traditionally attributed to neuronal loss of *Mecp2*, the effect of AE2 cell-specific *Mecp2* deficiency was compared with

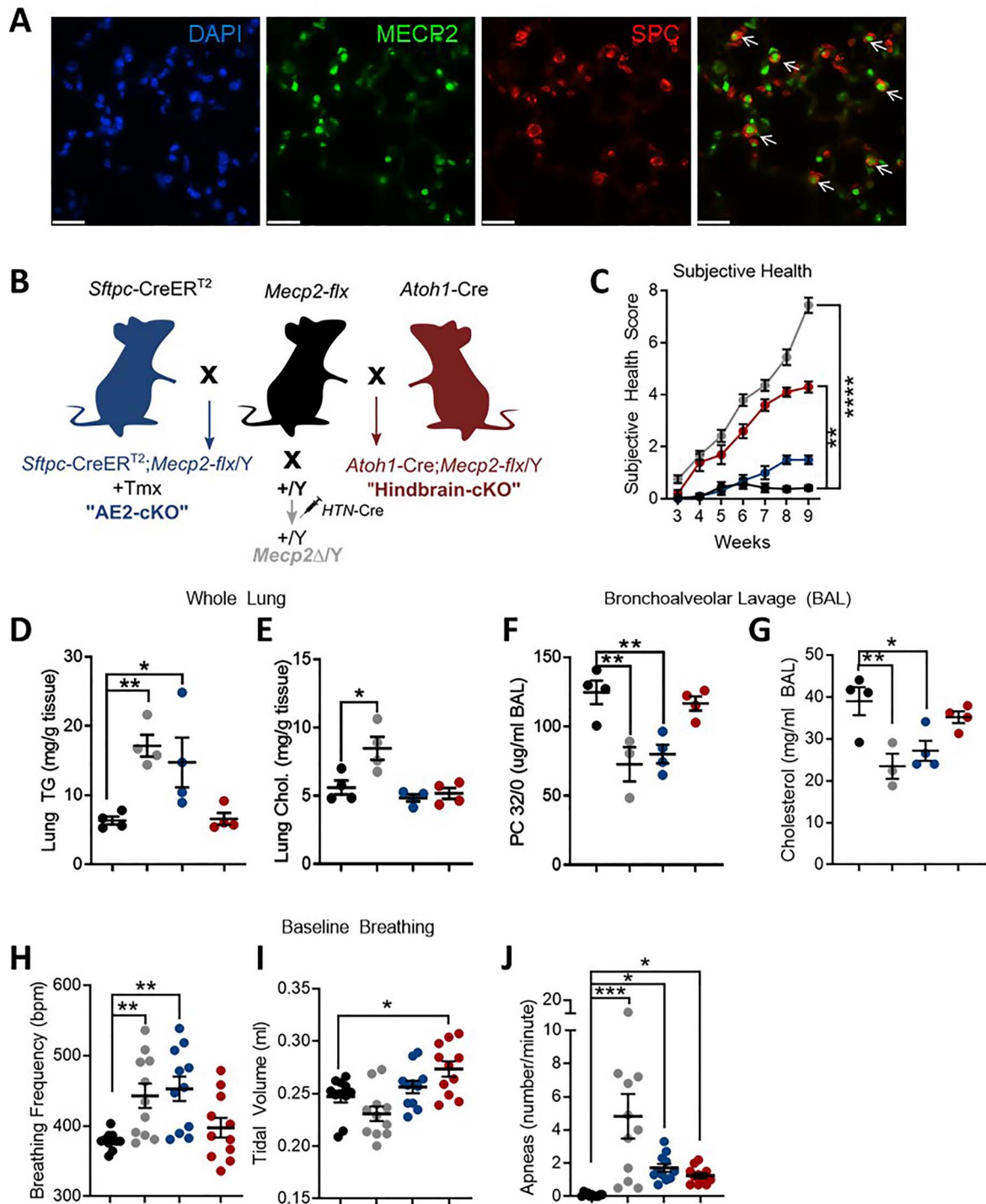


Figure 2. Conditional deletion of *Mecp2* in lung AE2 cells causes lipid accumulation and respiratory symptoms. (A) Lungs of *Mecp2^{tm3.1Bird}* mice were used to assess MECP2's localization. Blue: DAPI, green: GFP (MECP2), red: surfactant protein C [SPC, marker of alveolar epithelial 2 (AE2) cells]. Scale bars represent 40 μ m, arrows point to AE2 cells expressing MECP2. (B) Breeding scheme: B6.*Sftpc^{tm1(cre/ERT2)Bih}* (*Sftpc-CreER^{T2}*) or B6.Cg-Tg(*Atoh1-cre*)1Bfri (*Atoh1-Cre*) mice were used to achieve lung AE2 cell (AE2-cKO) or hindbrain neuron-specific (hindbrain-cKO) deletion of *Mecp2*. +/Y and *Mecp2 Δ /Y* mice were bred for comparisons. All littermates produced by breeding served as controls (Supplementary Material, Figs S3 and S4). (C) Subjective health scores, n=28 for +/Y, n=26 for *Mecp2/Y* (n=18 at P63 due to death), n=10 for hindbrain-cKO and lung-cKO. HPLC or LC/MS-MS analysis of (D) lung triglycerides, (E) lung cholesterol, (F) BAL PC 32/0 (DPPC) and (G) BAL cholesterol, n=4. Plethysmography analysis of (H) breathing frequency, (I) tidal volume and (J) apneas, n=11 per group. Data are expressed as mean \pm SEM. Statistics were performed using one-way ANOVA with Tukey's test for multiple comparisons. *P < 0.05, **P < 0.01, ***P < 0.001.

a neuron-specific deletion in the hindbrain, the site of neuronal control of respiration (Fig. 2B). *Mecp2* was removed from AE2 cells

by breeding B6.*Mecp2^{tm1Bird}* (*Mecp2-flx*) mice to B6.*Sftpc^{tm1(cre/ERT2)Bih}* mice, which express Cre under a tamoxifen (Tmx)-inducible

promoter of the surfactant protein C (*Sftpc*) gene, resulting in *Sftpc*-CreER^{T2}; *Mecp2*-flx conditional knockout ('AE2-cKO') mice. *Sftpc* is expressed exclusively in AE2 cells. *Mecp2* was deleted from hindbrain neurons using Cg-Tg(*Atoh1*-cre)1Bfr mice, which express Cre under the promoter of atonal basic helix loop helix (BHLH) Transcription Factor 1 (*Atoh1*). The resulting *Atoh1*-Cre; *Mecp2*-flx ('hindbrain-cKO') mice lack *Mecp2* in the medulla oblongata and pons, the respiratory centers of the brain responsible for maintaining respiratory rhythm. As a final control, B6.*Mecp2*-null (*Mecp2* Δ /Y) mice were generated by treating B6.*Mecp2*^{tm1Bird} embryos with a ubiquitously expressed Cre recombinase. Male C57BL/6 mice were used in this experiment, allowing the assessment of lung lipids on a second genetic background as previous experiments were carried out on the 129S6/SvEv genetic background. Tissue-specific deletion and reduced *Mecp2* expression was confirmed by polymerase chain reaction (PCR) (Supplementary Material, Fig. S2A).

As MECP2 deficiency causes neurological disease, neurobehavioral phenotypes were assessed through subjective health scoring (Fig. 2C), rotarod performance, open field behavior and social interaction (Supplementary Material, Fig. S2B–F). As expected, *Mecp2* Δ /Y mice develop neurobehavioral phenotypes, whereas AE2-cKO do not. Hindbrain-cKO have increased subjective health scores and deficits in motor coordination (Fig. 2C, Supplementary Material, Fig. S2B–F). Whole lung, BAL fluid and serum lipids were also measured. At P70, AE2-cKO mice show a significant increase in lung TGs (Fig. 2D, 6.86 ± 0.57 in +/Y; 14.76 ± 3.59 mg/g in AE2-cKO, $P=0.043$), along with a decrease in BAL fluid PC 32/0 (Fig. 2F, 124.59 ± 8.51 in +/Y; 80.14 ± 6.72 in AE2-cKO, $P=0.0087$) and BAL fluid cholesterol (Fig. 2G, 38.99 ± 3.33 in +/Y; 27.14 ± 2.39 in AE2-cKO, $P=0.030$). However, they do not have altered serum TGs or cholesterol (Supplementary Material, Fig. S2G–H, $P>0.05$). *Mecp2* Δ /Y mice have the same altered lung lipid profile as AE2-cKO mice; however, they also have increased lung cholesterol (Fig. 3E, 5.61 ± 0.55 in +/Y; 8.49 ± 0.84 in *Mecp2* Δ /Y, $P=0.015$), as well as increased serum TGs and cholesterol (Supplementary Material, Fig. S2G–H). In contrast, hindbrain-cKO mice do not show any changes in lung, BAL fluid or serum lipids ($P>0.05$). No significant changes were found in any parameters across littermate controls of AE2-cKO and hindbrain-cKO mice (Supplementary Material, Figs S3 and S4).

To assess respiratory symptoms, we used whole-body plethysmography (WBP), a non-invasive, quantitative method in which minute pressure changes in unrestrained mice are monitored and converted into respiratory waveforms. Compared with +/Y mice, both AE2-cKO and *Mecp2* Δ /Y mice have an elevated baseline breathing frequency (378.93 ± 3.6 breaths/min in +/Y, 442.93 ± 17.4 in *Mecp2* Δ /Y, $P=0.008$, and 452.77 ± 17.4 in AE2-cKO, $P=0.002$) (Fig. 2H). However, only hindbrain-cKO mice have an increase in tidal volume (0.24 ± 0.006 ml in +/Y; 0.27 ± 0.007 in hindbrain-cKO, $P=0.02$) (Fig. 2I). Thus, *Mecp2* deficiency in the lung and hindbrain may impart distinct respiratory symptoms. Apneas are the most characteristic respiratory symptom of RTT patients. Both AE2-cKO and hindbrain-cKO show a significant increase in the number of apneas produced (1.71 ± 0.24 apneas/min, $P=0.0002$ and 1.25 ± 0.15 , $P=0.004$, respectively), though apneas in *Mecp2* Δ /Y mice are far greater (0.08 ± 0.03 apneas/min in +/Y; 4.82 ± 1.34 in *Mecp2* Δ /Y, $P<0.0001$) (Fig. 2J). Thus, as loss of *Mecp2* in either AE2 cells or the hindbrain is sufficient to cause apneas, MECP2 may act in lung- and hindbrain-autonomous processes to regulate breathing; the combined loss of MECP2 from both centers likely imparts the full spectrum of respiratory symptoms in RTT.

Loss of *Mecp2* from lung alveolar cells alters lipogenic gene expression

The data presented thus far support the idea that altered lipids in AE2 cells contribute to respiratory symptoms in mouse models of *Mecp2* deficiency. Altered lipids could be a direct result of the inability to regulate lipid production upon loss of MECP2. In the liver, loss of *Mecp2* increases the transcription of lipogenesis genes through loss of NCOR1/2 binding (30). Thus, we hypothesized that MECP2 regulates lipid metabolism enzymes in lung AE2 cells. To identify genes that are misregulated in *Mecp2* deficiency, AE2 cells were isolated from P18 +/Y and *Mecp2*/Y mouse lungs by flow cytometry for single-cell RNA sequencing analysis (Supplementary Material, Fig. S5A). A pre-symptomatic time point was chosen with the aim of identifying primary disease-causing transcriptional changes (Fig. 3A). A total of 436 significant differentially expressed genes were identified in *Mecp2*/Y AE2 cells (Supplementary Material, Table S1). Of these, 113 had increased expression and 323 had decreased expression. The top 20 genes with altered expression are highlighted in Figure 3B.

Many lipid metabolism genes were misregulated in *Mecp2*/Y AE2 cells (Table 1) and the expression of a subset of genes was confirmed by reverse transcription quantitative polymerase chain reaction (RT-qPCR) (Supplementary Material, Fig. S5B). The expression of hydroxymethylglutaryl-CoA synthase (*Hmgcs1*) is increased in *Mecp2*/Y AE2 cells. HMGCS1 catalyzes an early step in cholesterol biosynthesis, converting acetoacetyl-CoA to 3-hydroxy-3-methylglutaryl-CoA (HMG-CoA), suggesting cholesterol biosynthesis is increased, which is consistent with lipid quantification results in *Mecp2*/Y lungs. Acyl-coA thioesterase 1 (*Acot1*) is the second most significantly increased gene in *Mecp2*/Y AE2 cells [\log_2 fold change (FC): 1.13, P -value: $3.10E-123$]. Consistently, its family member *Acot2* is also expressed at high levels compared with +/Y cells. When required for energy or other metabolic processes, fatty acids are converted to acyl-CoAs by long-chain acyl-CoA synthetases (ACs) and transported to the mitochondria for beta-oxidation. Acyl-CoA thioesterases (ACOTs) catalyze the reverse reaction, and as such, ACs and ACOTs direct the metabolic fate of fatty acids by channeling substrates toward or away from beta-oxidation. These results suggest fatty acids in the *Mecp2*/Y lung are shuttled away from mitochondrial recycling and pushed toward lipid storage pathways. Consistent with previous literature on mitochondrial involvement in RTT (35–37), loss of *Mecp2* impacted electron transport chain (ETC) components, with 11 of the 13 mitochondrially expressed ETC components being expressed at lower levels in *Mecp2*/Y AE2 cells (Table 1).

Despite high levels of TGs in the *Mecp2*/Y lung, a global decrease in lipid biosynthesis gene expression was found. Fatty acid biosynthesis genes including fatty acid synthase (*Fasn*), stearoyl-CoA desaturase 1/2 (*Scd1,2*) and elongation of very long chain fatty acids (ELOVL) fatty acid elongase (*Elovl1*) are significantly decreased in single cell sequencing (sc-seq) data of *Mecp2*/Y AE2 cells at P18. Fatty acid transporters and TG hydrolases were unchanged in both AE2 cells and whole lung from *Mecp2*/Y mice, with the exception of lipoprotein lipase (*Lpl*), which was decreased in *Mecp2*/Y AE2s (Supplementary Material, Fig. S5C). Therefore, we assessed SREBPs, membrane-bound transcriptional regulators of lipid homeostasis (38,39). SREBPs are synthesized as inactive precursors bound to endoplasmic reticulum membranes. When lipid levels are low, SREBPs migrate to the nucleus and bind and activate the transcription of lipogenesis genes containing sterol response elements (SREs) in their promoters (40). In *Mecp2*/Y AE2 cells, the expression of *Sreb1*, which

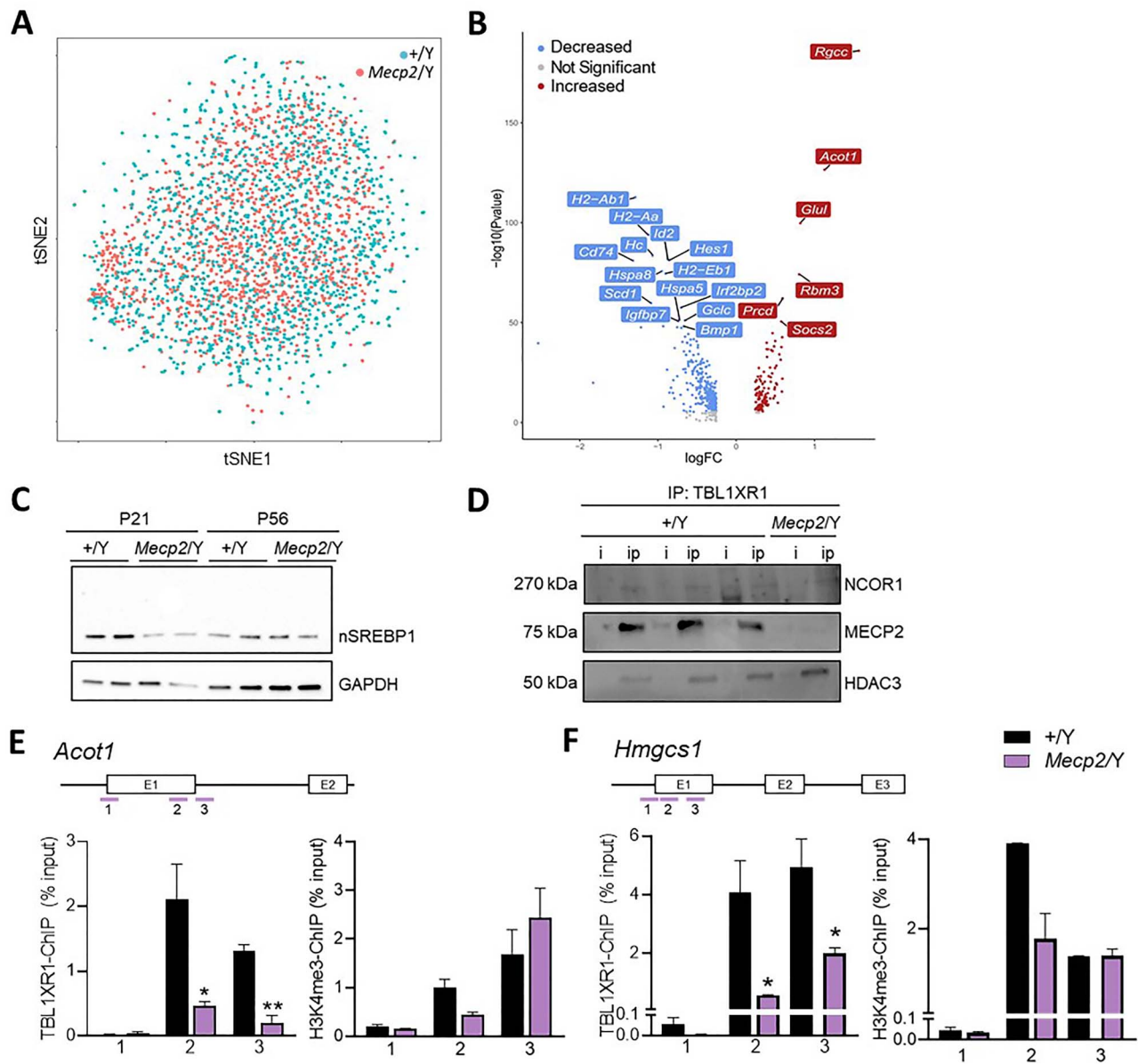


Figure 3. Metabolic genes are altered in *Mecp2/Y* AE2 cells due to loss of MECP2- and NCOR1/2-mediated transcriptional repression. (A) t-SNE plot of +/Y and *Mecp2/Y* AE2 cells after single-cell RNA sequencing, $n = 2000$ cells, collected at P18. (B) Volcano plot showing genes with altered expression in *Mecp2/Y* AE2 cells after single-cell RNA sequencing. The top 20 significantly altered genes are labeled. Significant genes have $-\log_{10}(\text{P-value}) < 0.05$. (C) SREBP1 expression in the +/Y and *Mecp2/Y* lung at P21 and P56. The 68 kDa band (shown) is the active, cleaved protein, whereas the 120 kDa inactive precursor was not visualized. GAPDH was used for normalization. (D) TBL1XR1 is associated with NCOR1/2 co-repressor complex members NCOR1, MECP2 and HDAC3 in the mouse lung, as shown by co-immunoprecipitation (co-IP) assay. This complex forms without MECP2 in *Mecp2/Y* lung tissue. i, input (nuclear protein); ip, immunoprecipitated protein. Anti-TBL1XR1 and anti-H3K4me3 (positive control) ChIP-qPCR of sites surrounding the (E) *Acot1* promoter and (F) *Hmgcs1* promoter, $n = 3$. Data are expressed as mean \pm SEM. Statistics were assessed using Student's t-test. * $P < 0.05$, ** $P < 0.01$. FC, fold change.

stimulates TG synthesis, is decreased, whereas *Srebf2*, which stimulates sterol synthesis, is unchanged. A western blot assay in whole lung tissue confirmed that nuclear SREBP1 expression is decreased at P21 but is normal by P56 (Fig. 3C). In contrast, nuclear SREBP2 expression is unchanged at both time points (Supplementary Material, Fig. S5D). SREBP1c transcriptionally activates the SRE-containing genes *Fasn*, *Scd1* (41), *Scd2* (42) and ATP citrate lyase (*Acly*) (43), which have decreased expression in *Mecp2/Y* AE2 cells.

PCs represent the largest percentage of lipids in pulmonary surfactant. Synthesis of PCs by the cytidine diphosphate (CDP):choline pathway begins with the uptake of exogenous choline from the bloodstream predominantly by sodium-

dependent choline transporters. Choline is phosphorylated by choline kinase (CK) to form phosphocholine, which is activated by cytidine triphosphate (CTP):phosphocholine cytidyltransferase (CCT) to make CDP-choline, which is finally joined to a diacylglycerol (DG) backbone by choline/ethanolamine phosphotransferase to form PC. In *Mecp2/Y* AE2 cells, the CK, choline kinase alpha (*Chka*) and the CPT, phosphate cytidyltransferase 1 choline alpha (*Pcyt1a*) are significantly underexpressed (*Chka* FC: -0.549 , P -value: $5.87E-22$; *Pcyt1a* FC: -0.262 , P -value: $3.77E-5$). The PC transporter *Abca3* is expressed at lower levels in *Mecp2/Y* AE2 cells (FC: -0.506 , P -value: $5.42E-9$). Mutations in *ABCA3* are associated with surfactant deficiency and fatal respiratory distress (44). Decreased expression of

Table 1. *Mecp2* deficiency alters lipid metabolism gene expression in lung AE2 cells

	Gene	Log FC (Down/Up)	P-value
Transcriptional regulation of lipid metabolism	<i>Cebpa</i>	↓ 0.66157	2.75E-32
	<i>Srebfl</i>	↓ 0.48646	1.58E-25
	<i>Nr1d1</i>	↓ 0.33904	2.18E-25
	<i>Foxa2</i>	↓ 0.29705	1.31E-11
Sterol biosynthesis	<i>Pmk</i>		↑ 0.34146 3.15E-16
	<i>Hmgcs1</i>		↑ 0.28520 2.45E-08
	<i>Soat1</i>	↓ 0.52903	9.72E-24
Fatty acid biosynthesis	<i>Raly</i>	↓ 0.25489	0.000109
	<i>Cyb5a</i>		↑ 0.33186 1.88E-10
	<i>Scd1</i>	↓ 1.08181	1.57E-56
	<i>Scd2</i>	↓ 0.74866	2.11E-44
	<i>Eloul1</i>	↓ 0.54825	2.27E-15
	<i>Fasn</i>	↓ 0.28478	5.45E-05
	<i>Acly</i>	↓ 0.35509	5.37E-11
	<i>Acot1</i>		↑ 1.13401 3.10E-123
Fatty acid regulation	<i>Eci2</i>		↑ 0.41057 2.34E-33
	<i>Acot2</i>		↑ 0.28115 6.12E-14
	<i>Acs15</i>	↓ 0.46970	1.78E-14
	<i>Plin2</i>		↑ 0.31851 2.27E-17
	<i>Chka</i>	↓ 0.54883	5.87E-22
Lipid storage	<i>Dgkg</i>	↓ 0.31762	7.60E-13
	<i>Lpcat1</i>	↓ 0.48220	2.39E-06
	<i>Pcyt1a</i>	↓ 0.26249	3.77E-05
	<i>Sptlc2</i>	↓ 0.37772	2.04E-14
Phospholipid biosynthesis	<i>Sgms1</i>	↓ 0.32411	1.33E-09
	<i>Cd74</i>	↓ 1.31228	9.21E-78
	<i>Cftr</i>	↓ 0.27103	5.74E-11
Sphingolipid synthesis	<i>Mlc1</i>	↓ 0.36050	4.80E-09
	<i>Prdx6</i>		↑ 0.59145 2.18E-39
	<i>Gpx1</i>		↑ 0.58170 1.92E-34
	<i>Acox1</i>	↓ 0.56540	4.54E-27
Mitochondria (nuclear)	<i>Ndufa6</i>		↑ 0.55456 8.27E-31
	<i>Ndufa7</i>		↑ 0.29279 2.91E-09
	<i>Uqcrh</i>		↑ 0.29871 4.72E-11
	<i>Cox7a2L</i>		↑ 0.29685 6.65E-10
	<i>Ndufa3</i>	↓ 0.28295	0.000335
Mitochondria (mt-expressed)	<i>mt-nd1</i>	↓ 0.84693	1.21E-11
	<i>mt-nd2</i>	↓ 0.87795	3.75E-23
	<i>mt-nd3</i>	↓ 0.92690	6.98E-45
	<i>mt-nd4l</i>	↓ 0.25441	0.006614
	<i>mt-nd4</i>	↓ 0.82727	3.84E-14
	<i>mt-nd5</i>	↓ 0.57768	2.96E-16
	<i>mt-cyb</i>	↓ 0.66476	5.31E-06
	<i>mt-co1</i>	↓ 0.53783	0.046432
	<i>mt-co2</i>	↓ 0.80265	1.68E-11
	<i>mt-co3</i>	↓ 0.78379	8.45E-09
	<i>mt-atp6</i>	↓ 0.58252	0.022863

Genes are classified by lipid metabolism pathway and sorted by P-value. LogFC, Log₂ fold change.

PC-producing enzymes is likely responsible for the remarkably low levels of PCs in *Mecp2*/Y BAL fluid. Notably, *Pcyt1a* and *Abca3* are major targets of SREBP-induced activation (7,45); therefore, increased TGs could inadvertently reduce SREBP activity, limiting PC synthesis.

MECP2 regulates the expression of lung lipid metabolism enzymes through interaction with the NCOR1/2 co-repressor complex

The NCOR1/2 complex includes HDAC3, G protein pathway suppressor 2, TBL1X and TBL1XR1, the latter of which are direct

binding partners of MECP2. NCOR1 and HDAC3 are master regulators of lipid biosynthesis in the liver (28,29). We previously showed that decreased binding of NCOR1/2 in a state of MECP2 deficiency leads to the upregulation of lipid biosynthesis genes in the liver (30). In mouse lung, co-immunoprecipitation of TBL1XR1 revealed an association with MECP2, as well as with NCOR1/2 co-repressor complex partners NCOR1 and HDAC3 (Fig. 3D). The formation of this complex in the lung suggests its role in the direct regulation of lipid metabolism gene targets.

As the MECP2-NCOR1/2 complex primarily acts as a transcriptional repressor, genes with increased expression in *Mecp2*/Y AE2 cells were chosen as putative targets of

MECP2-directed transcriptional regulation for chromatin immunoprecipitation (ChIP)-qPCR. ChIP was performed using an anti-TBL1XR1 antibody. Histone 3 lysine 4 trimethylation (H3K4me3) and immunoglobulin G (IgG) (Supplementary Material, Fig. S5E and F) were assessed as positive and negative controls, respectively. Loss of *Mecp2* significantly hinders the binding of TBL1XR1 to *Acot1* (Fig. 3E) and *Hmgcs1* (Fig. 3F), both of which have increased expression in *Mecp2/Y* AE2 cells. These results suggest that MECP2, in concert with the NCOR1/2 co-repressor complex, directly regulates the expression of *Acot1* and *Hmgcs2* in the mouse lung. In contrast, TBL1XR1 does not bind to the promoter region of the peroxiredoxin-6 (*Prdx6*) gene, which is also expressed at high levels in *Mecp2/Y* AE2 cells (Supplementary Material, Fig. S5G).

Fluvastatin treatment reduces lung TG accumulation and improves breathing symptoms in male *Mecp2/Y* mice

As aberrant lung lipids likely contribute to respiratory symptoms in *Mecp2*-mutant mice, we sought to test the effects of pharmacological correction of lung lipid metabolism. Statins are commonly prescribed pharmaceuticals that reduce systemic cholesterol and TGs by interfering with lipid metabolism through competitive inhibition of HMG-CoA-reductase. Previously, two classes of statins, lovastatin and fluvastatin, were shown to improve overall health, motor activity and metabolic health in 129.*Mecp2*-mutant mice (33). A second study found that lovastatin was unable to improve these parameters in B6.*Mecp2/Y* mice (46). As lovastatin is very labile and requires careful activation and handling for its use in mice, fluvastatin was used in this study.

Weekly fluvastatin treatment reduced serum lipids in *Mecp2/Y* mice while improving subjective health scores and motor coordination, as previously shown (33) (Fig. 4A, Supplementary Material, Fig. S6A–D). It also lowered lung TGs (Fig. 4B), but lung cholesterol was unchanged across all groups (Fig. 4C). Remarkably, fluvastatin treatment normalized breathing frequency in *Mecp2/Y* mice and modestly, but not significantly, improved respiratory apneas (Fig. 4D–F).

Therefore, to validate the therapeutic relevance of metabolism-targeted treatment for human RTT patients, the effects of statin treatment on respiratory symptoms in female 129.*Mecp2*^{tm1.1Bird}/+ mice were assessed (Fig. 4G). Fluvastatin treatment reduced serum cholesterol and improved subjective health scores and rotarod performance in *Mecp2/+* mice, as previously shown (33) (Supplementary Material, Fig. S6E–H). Fluvastatin treatment also lowered lung TG levels in *Mecp2/+* mice (4.14 ± 0.9 mg/g in vehicle-treated +/+, 14.70 ± 3.01 in vehicle-treated *Mecp2/+*; 7.54 ± 0.72 in treated *Mecp2/+*, $P=0.0229$) (Fig. 4H). Lung cholesterol was unchanged across the four groups (Fig. 4I). Thus, low doses of fluvastatin improve aberrant lipid accumulation. Fluvastatin treatment also normalized breathing frequency in *Mecp2/+* mice compared with vehicle-treated *Mecp2/+* mice (273.01 ± 8.93 breaths/min in fluvastatin-treated *Mecp2/+*; 316.81 ± 13.77 in vehicle-treated *Mecp2/+*, $P=0.046$; 273.03 ± 10.42 in vehicle-treated +/+, Fig. 4J) as it did in male mice. Fluvastatin treatment did not affect tidal volume, which was unchanged in *Mecp2/+* mice (Fig. 4K). Despite female *Mecp2/+* mice having a lower occurrence of respiratory apneas than their male counterparts, fluvastatin treatment remarkably restored respiratory apnea counts (0.2 ± 0.06 apneas/min in vehicle-treated *Mecp2/+*; 0.04 ± 0.02 in fluvastatin-treated

Mecp2/+, $P=0.012$) to wild-type levels (0.023 ± 0.02 in vehicle-treated +/+) (Fig. 4L). Therefore, statin treatment can lower lung lipids and improve respiratory symptoms in mouse models of RTT.

Discussion

RTT research has historically focused on the role of *Mecp2* in the central nervous system. However, patient symptoms as well as phenotypes in *Mecp2*-mutant mice suggest important roles for *Mecp2* outside of the brain. Here, we show for the first time that *Mecp2* deficiency in mice results in lung lipid perturbations; neutral lipids accumulate in the lung, whereas surfactant phospholipids drastically decrease. Such a marked reduction in surfactant PCs will impact surfactant function and reduce the lung's capacity to facilitate normal gas exchange. Impaired surfactant function is a key feature of many respiratory disorders (1,3,44); therefore, surfactant deficiency could contribute to the hallmark respiratory symptoms of RTT. Importantly, misregulated lung lipid metabolism in *Mecp2*-mutant mice results from loss of transcriptional regulation by the NCOR1/2 co-repressor complex due to *Mecp2* deficiency. AE2 cell-specific deletion is sufficient to cause lung lipid abnormalities that lead to respiratory anomalies in mice. Respiratory symptoms improve in *Mecp2*-mutant mice with statin treatment, consistent with the findings that aberrant lung lipids contribute to respiratory disturbances. These findings provide mechanistic evidence for the respiratory defects in RTT and have important translational value for patients.

MECP2 directs lipid metabolism with the NCOR1/2 co-repressor complex, resulting in abnormal lung surfactant components

Mecp2/Y mouse lungs have a global perturbation of lung lipid metabolism, which is also present in female *Mecp2/+* mice, suggesting heterozygous mosaic loss of *Mecp2* is sufficient to alter lung lipids. Lipid metabolism abnormalities are evident in *Mecp2*-mutant mouse models and RTT patients. Symptomatic *Mecp2/Y* male mice have increased brain cholesterol, serum cholesterol and TGs, and develop fatty liver disease (30,33). A subset of RTT patients has increased serum cholesterol and TGs (47,48).

MECP2 is required for the NCOR1/2 co-repressor complex to bind to a subset of its gene targets, although these targets may differ across different tissues. As a master regulator of metabolism, a direct target of the MECP2-NCOR1/2 complex in the liver is squalene epoxidase (*Sqle*), a rate-limiting enzyme in cholesterol synthesis (30,47). In *Mecp2/Y* AE2 cells, the NCOR1/2 complex protein TBLX1R1 does not readily bind to *Acot1* and *Hmgcs1* genes, which are consistently expressed at higher levels (Fig. 5A), suggesting that they are direct targets of this repressor complex. ACOT1 is essential for directing the metabolic fate of fatty acids and its upregulation suggests decreased substrate production for beta-oxidation by shuttling fatty acids away from degradation. HMGCS1 produces HMG-CoA, the substrate for the first rate-limiting step of cholesterol biosynthesis. Importantly, much of the lung's cholesterol content is derived from the serum; therefore, increased serum cholesterol in *Mecp2/Y* mice may contribute to the lung cholesterol phenotype shown here. However, BAL fluid cholesterol, made exclusively by AE2 cells, is increased at P21 in *Mecp2/Y* mice, and lung TGs are elevated in AE2-cKO mice, in spite of the lack of elevated serum lipids. Similarly, BAL fluid PCs are decreased in AE2-cKO mice, suggesting

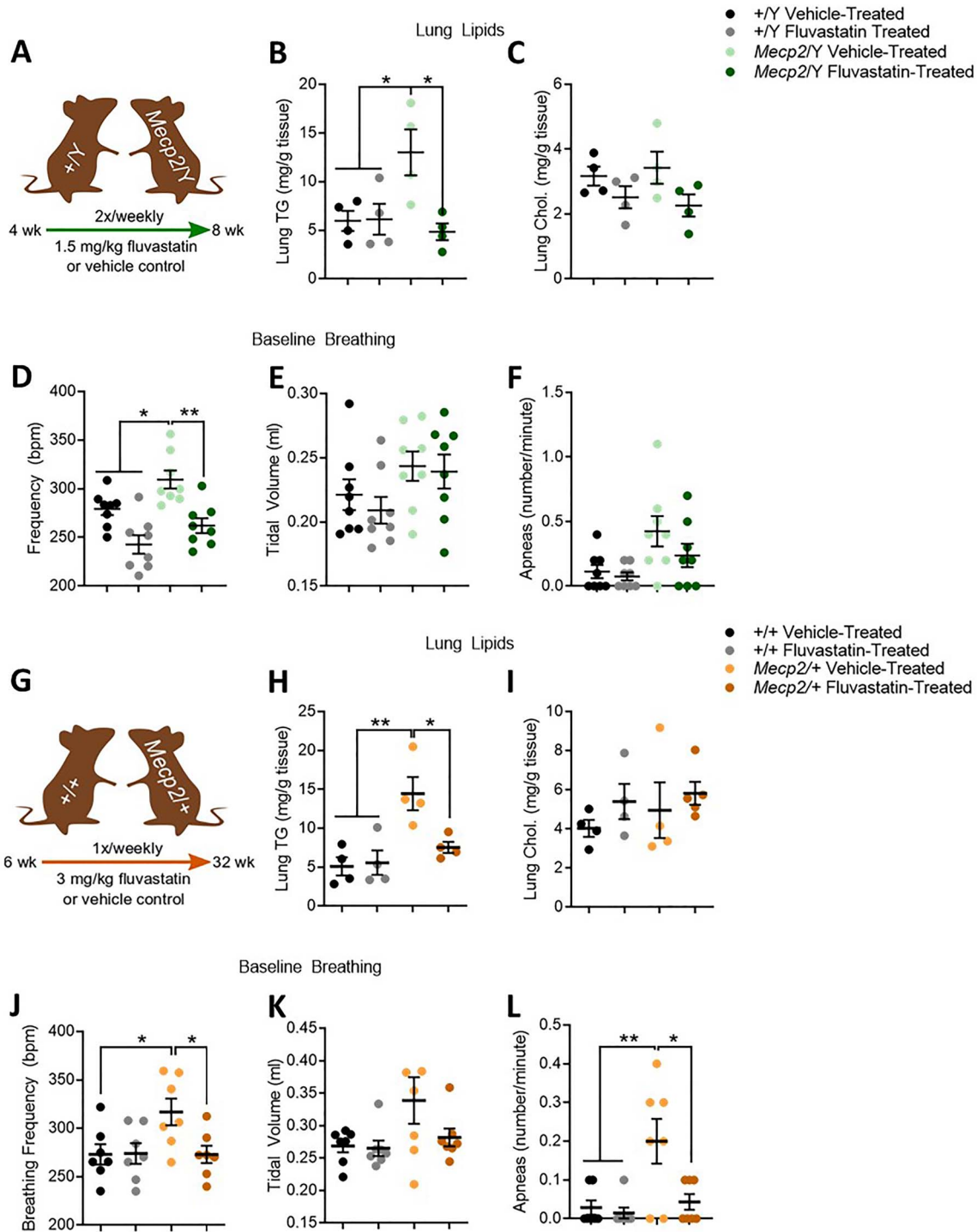


Figure 4. Fluvastatin treatment reduces lung lipids and improves respiratory symptoms in *Mecp2*-mutant mice. (A) Male mice were administered fluvastatin or vehicle control from 4 to 8 weeks of age. HPLC analysis of lung (B) triglycerides and (C) cholesterol, $n=4$. Respiratory parameters were measured: (D) breathing frequency, (E) tidal volume and (F) apneas, $n=8$. (G) Female mice were administered fluvastatin or vehicle control from 6 to 32 weeks of age. HPLC analysis of lung (H) triglycerides and (I) cholesterol, $n=4$. Respiratory parameters were measured: (J) breathing frequency, (K) tidal volume and (L) apneas, $n=7$. Data are expressed as mean \pm SEM. Statistics were performed using one-way ANOVA with Tukey's test for multiple comparisons. * $P < 0.05$, ** $P < 0.01$, *** $P < 0.001$.

decreased surfactant PCs and excess lung TGs are mechanistically linked. DGs are required for PC synthesis and are incorporated via phospholipid:diacylglycerol acyltransferase enzymes; the reverse reaction reduces the pool of PCs to make DGs, which become TGs via diglyceride acyltransferase (DGAT) enzymes.

Although these genes were not identified in our single-cell RNA sequencing experiment, it is likely that loss of MECP2's transcriptional repression at other genes that regulate lipid homeostasis via the NCOR1/2 co-repressor complex alter lipid biosynthesis and storage in the *Mecp2*-deficient lung. Identifying other

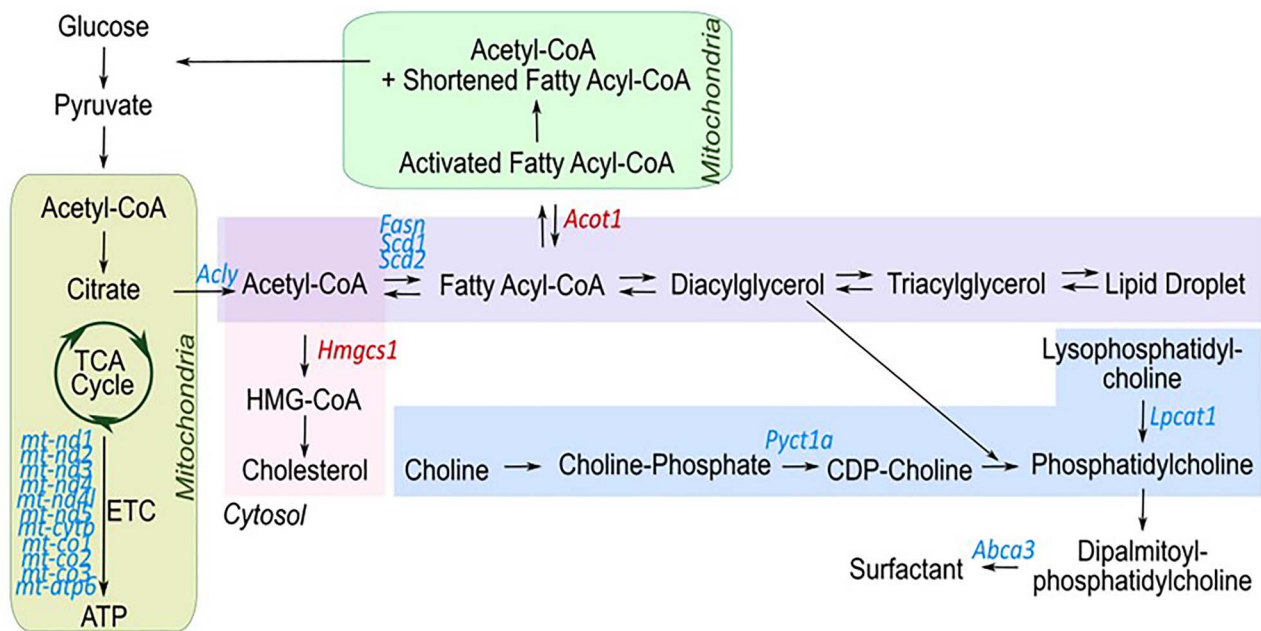


Figure 5. Putative mechanism for altered lung lipid metabolism in *Mecp2/Y* cells. Schematic of genes in lipid synthesis pathways, highlighting genes with altered expression in *Mecp2/Y* AE2 cells based on single-cell RNA sequencing. All genes shown have altered gene expression with a *P*-value <0.05. Arrows indicate direction of metabolic reaction. Genes in red are targets of NCOR1/2-mediated repression. Cytoplasmic genes in blue have decreased expression in *Mecp2/Y* AE2 cells and are potential targets of SREBPs. Mitochondrial genes in blue have reduced expression in *Mecp2/Y* AE2 cells and may be altered downstream of other metabolic changes.

lipid-regulating targets of MECP2 in AE2 cells, and other cells in the lung, will be necessary for a full understanding of the cause of lung lipid abnormalities.

The drastic reduction of surfactant PCs in *Mecp2*-mutant mice is an important finding. Single-cell RNA sequencing revealed that *Chka* and *Pyc1a*, two key enzymes of the PC synthesis pathway, are underexpressed. It is possible that loss of MECP2 may indirectly shut down PC synthesis through SREBP1, preventing normal surfactant production (Fig. 5). Another possibility is that TGs are shuttled toward storage, reducing the pool of DGs for PC synthesis. In addition, as BAL fluid PCs, but not lung PCs, are significantly decreased, surfactant exocytosis could be deficient, trapping PCs in AE2 cells. The resolution of these possibilities will require further exploration. Changes in phospholipid composition in the lung surfactant of *Mecp2*-deficient animals alone could be a major driving force of the respiratory symptoms associated with RTT. Reduced surfactant PCs cause surfactant dysfunction and impair the lung's ability to facilitate gas exchange. In addition, *in vitro* experiments have shown that excess cholesterol and/or neutral lipids disrupt the surface tension-lowering capability of surfactant (49). Notably, surfactant dysfunction causes ground glass opacities and bronchial thickening in computed tomography scans, both of which are present in RTT patient lungs (50).

Respiratory symptoms upon *Mecp2* deletion are a result of lung- and brain-autonomous events

The comparison of respiratory symptoms in mice with AE2 cell-specific depletion of *Mecp2* to mice with a hindbrain neuron-specific deletion of *Mecp2* revealed that AE2 cell-specific loss of *Mecp2* elevated lung TGs, reduced BAL fluid PCs and caused respiratory symptoms. These findings demonstrate that loss of *Mecp2* in the lung directly contributes to respiratory symptoms

in RTT, challenging the view that RTT symptoms result solely due to neuron-specific loss of *Mecp2* (51).

Breathing frequency was increased in mice with an AE2-cell deletion of *Mecp2*, whereas tidal volume was changed in mice with a hindbrain neuron-specific deletion of *Mecp2*, suggesting loss of *Mecp2* from either the lung or hindbrain imparts distinct respiratory symptoms. Respiratory apneas are considered the most striking respiratory symptom of RTT as they can lead to cyanosis and fainting (52). Intriguingly, mice with AE2 cell-specific and hindbrain neuron-specific deletions of *Mecp2* both display an elevation in the number of respiratory apneas. However, apneas in *Mecp2Δ/Y* mice were far more severe. Our data suggest that both neuronal- and lung-autonomous processes influence respiratory apneas, and loss of *Mecp2* from both areas likely acts in an additive manner to produce the dramatic apneas evidenced in RTT patients and *Mecp2*-mutant mouse models.

Lung metabolic defects impact long-term patient care

Here, we show that *Mecp2* is a crucial regulator of lipid metabolism in the lung, and that its loss imparts consequences on lung homeostasis and respiratory symptoms. RTT patient death is most often caused by lung infection, asphyxiation and respiratory failure (11), and at least 17% of RTT patients develop pneumonia (52). Surfactant proteins bind to pathogens and facilitate their clearance by alveolar macrophages (49); surfactant deficiency or dysfunction can therefore weaken the lung's immune response to foreign pathogens. In addition, accumulated lung lipids can interfere with macrophage clearance efforts, thereby decreasing their efficacy in preventing infection (53). Low doses of fluvastatin improve lung lipid accumulation and respiratory symptoms in both male and female *Mecp2*-mutant mice. TGs are the primary elevated lipid in the *Mecp2*-deficient lung. Statins, while an HMGCR inhibitor, reduce serum

TGs, which may increase TG secretion from tissues, reducing their lipid storage pools. It is a possibility that the lung has reduced uptake of fatty acids from the serum; however, the AE2-cKO model has increased lung TGs in the absence of increased serum lipids, ruling out this possibility. Although BAL fluid lipids were not measured in statin-treated *Mecp2*-mutant mice, these findings raise the possibility that systemic treatment of lipid metabolism could regulate surfactant PCs, ultimately improving surfactant efficacy. Reducing lung lipids with statins could restore surfactant function in RTT patients, preventing further respiratory ailments.

These results extend and confirm that MECP2 acts with the NCOR1/2 complex as a regulator of metabolism in multiple tissues. The role of lung metabolism in respiratory illness should now be monitored by physicians when evaluating RTT patients. Lung perturbations should also be considered in studies of *Mecp2*-mutant mice. Importantly, lipid metabolism is highly targetable through pharmaceutical drugs; lipid-lowering therapeutics may be efficacious in improving respiratory abnormalities and maintaining lung health in RTT patients.

Materials and Methods

Animals

All animal procedures were approved under animal use protocol 21-0251H by the Animal Use Committee at the Canadian Council on Animal Care (CCAC)-accredited animal facility, The Center for Phenogenomics (TCP). Congenic 129.*Mecp2*^{tm1.1Bird}/Y mice feature a deletion of the last two exons (exons 3–4) of the *Mecp2* transcript, resulting in a null allele. Male *Mecp2*/Y (null) and +/Y (wild type), and female *Mecp2*/+ and +/- mice were obtained by backcrossing *Mecp2*^{tm1.1Bird}/+ females to males of the 129SvEvS6/Tac strain for >10 generations. Mice were fed a standard diet (Harlan Teklad 2918) ad libitum, consisting of 18% protein, 6% fat and 44% carbohydrates. Mice were housed in a 12 h light/dark cycle and were euthanized between the hours of 9 a.m. and 12 p.m. (ZT 2–5) to control for circadian rhythm fluctuations. 129.*Mecp2*/Y male mice develop behavioral phenotypes, including hindlimb clasp and hypoactivity, at 4 weeks of age, followed by a rapid decline in health and death by 8–10 weeks. 129.*Mecp2*/+ female mice develop neurological phenotypes between 4 and 6 months of age with symptom variability due to random X-chromosome inactivation.

Conditional deletions of *Mecp2*, and respective controls, were obtained by crossing B6.*Mecp2*^{tm1Bird}/+ (*Mecp2*-flx) heterozygous female mice to male mice heterozygous for Cre transgenes, which were also on a C57BL/6J background. AE2 cell-specific deletion of *Mecp2* was achieved by crossing *Mecp2*-flx mice to B6.*Sftpc*^{tm1(cre/ERT2)Blh} mice, which have a Tmx-inducible Cre under the control of the surfactant protein C promoter. *Sftpc*^{tm1(cre/ERT2)Blh}; *Mecp2*^{tm1Bird}/Y (AE2-cKO) mice were given three 75 mg/kg bodyweight intraperitoneal injections of Tmx at 3 weeks of age over a period of 5 days (every other day) to induce Cre excision. Hindbrain-specific deletion of *Mecp2* was achieved by crossing *Mecp2*-flx mice to mice with Cre under the control of the atonal BHLB transcription factor 1 promoter (B6.Cg-Tg(Atoh1-cre)1Bfri). *Atoh1* regulatory elements drive constitutive Cre expression in precursors of granule cell neurons of the cerebellum, dorsal hindbrain and spinal cord (hindbrain-cKO). To achieve whole-body deletion of *Mecp2* on the C57BL/6J background, two-cell embryos were retrieved from pregnant *Mecp2*^{tm1Bird}/+ mice, incubated in a solution containing Histidine-Transactivator of transcription (TAT)-Nuclear localization signal-tagged Cre

recombinase and transferred to a pseudo-pregnant female recipient, as previously described (54), by the Mouse Model Services Core at TCP. Female C57BL/6 *Mecp2*^{tm3.1Bird} mice were obtained from The Jackson Laboratory. These mice harbor a knock-in mutation of an Enhanced Green Fluorescent Protein (EGFP) sequence in the 3'UTR of the *Mecp2* gene. Female *Mecp2*^{tm3.1Bird} mice were bred to wild type male mice to produce male *Mecp2*^{tm3.1Bird} offspring.

Electron microscopy and immunohistochemistry

Mice were anesthetized with an intraperitoneal injection of 100 mg/kg bodyweight of ketamine and 10 mg/kg bodyweight xylazine in saline. Once unresponsive, a needle was inserted into the left ventricle of the heart and mice were perfused with 10 U/ml heparin in phosphate-buffered saline (PBS) at a rate of 3 ml/min for 10 min. Lungs were fixed via intratracheal administration of 2.5% glutaraldehyde in 0.1 M phosphate buffer (pH 7.4). The trachea was tied with sutures and the lung was dissected out of the chest cavity and immersed in the above fixative for 16 h at 4°C. Tissues were post-fixed in osmium tetroxide, dehydrated in an ascending series of acetone and embedded in Epon Araldite prior to polymerization at 60°C overnight. Thin sections were cut, mounted on grids, and stained with uranyl acetate and lead citrate prior to microscopy. Images were captured with a charge-coupled device camera (AMT Corp.) and an electron microscope (JEOL JEM1011). A minimum of 15 images were taken from each animal.

For immunohistochemistry, lungs of P21 *Mecp2*^{tm3.1Bird} mice were perfused with 10 U/ml heparin in PBS as above and fixed via intratracheal administration of 4% paraformaldehyde (PFA). Excised lungs were immersed in 4% PFA for 16 h at 4°C. Tissues were washed in PBS, embedded in paraffin, cut at a thickness of 5 µm and dried on a slide warmer at 37°C. Mounted sections were deparaffinized in a graded series of ethanol washes. Antigen retrieval was performed in 0.01 M citrate buffer, pH 6.0. Slides were blocked with 5% goat serum, 1% bovine serum albumin and 0.1% Triton X-100 in PBS. Slides were incubated with primary and secondary antibodies: GFP (ab13970, 1:500), surfactant protein C (SPC) (ab90716, 1:500), Alexafluor 488 (Thermo A-11039, 1:400), Alexafluor 594 (Thermo A-11012, 1:400). Slides were mounted using ProLong Gold Antifade Mount with 4',6-diamidino-2-phenylindole (DAPI) (Thermo Fisher) and imaged on a Nikon A1R confocal laser microscope equipped with NIS Elements analysis software. For histology, lungs were perfused as described above. A mixture of 1:1 optimal cutting temperature compound and PBS was administered intratracheally. Excised lungs were immersed in a cryo mold and frozen on dry ice. Sections were sliced using a cryostat and oil red O stain was applied.

Lipid analysis

Blood was drawn from mice using cardiac puncture between the hours of 2 p.m. and 5 p.m. (ZT 7–10) and serum was separated in BD serum separation tubes following manufacturer instructions. Serum and tissue samples were stored at –80°C until analysis by the Diabetes and Endocrinology Center at Baylor College of Medicine (Houston, TX). Lipids were isolated from tissue using CHCl₃:CH₃OH extraction, followed by drying of the organic phase under N₂ pressure. Serum and tissue cholesterol and TG concentrations were assessed by HPLC.

After sacrifice, a blunt tip 20 G needle was inserted into the trachea and the lungs were lavaged with sterile PBS (500 µl

for P21 mice and 1 ml for mice P56 or older; retrieval volume was generally 75–80% of administration volume). BAL fluid was stored at -80°C until further processing. Measurements of BAL cholesterol and PC were performed by LC-MS/MS at the Analytical Facility for Bioactive Molecules at The Hospital for Sick Children (Toronto, Canada). BAL samples (200 μl) were transferred to siliconized glass tubes containing 800 μl of ultra-pure water and were spiked with internal standards. Lipid extraction was performed using chloroform/methanol extraction. Organic phases were dried and reconstituted in 100 μl ethanol with 0.2% formic acid and transferred to siliconized vials for analysis. LC/MS-MS was performed on an Agilent 1290 Series binary pump (Agilent Technologies Inc.) coupled to an API4000 triple-quadrupole mass spectrometer (SCIEX). Quantitative analyses were based on the calibration curve for each analyte and analyzed by LC/MS-MS in the same conditions.

Subjective health assessments

Mice were assayed for general health once per week from 4 to 10 weeks of age. Scoring was blinded by genotype. Mice were scored using a published assessment method with slight modifications (33,55). In this scoring method, mice are given a score between 0 and 2 based on the severity of the phenotype assessed (Supplementary Material, Table S2). Mice were assessed for limb claspings, tremors, activity, grooming, hypotonia and body weight, for a combined possible score of 0–12.

Rotarod

Motor coordination was measured using the rotating rod (Stoelting Ugo Basile Mouse Rota-Rod). Mice were placed on the grooved rotating rod facing the opposite direction of rotation. The revolution rate increased from four rotations per minute (RPM) to 40 RPM over the course of 5 min. The length of time that each mouse remained on the rod was recorded for eight trials over two consecutive days (four trials per day), with a minimum of 30 min between each trial. A trial ended for a mouse when it fell from the rod, stayed stationary on the rod while it spun for two revolutions, or when it successfully stayed on the rod for 5 min.

Open field activity

Locomotor activity was measured by free activity in an open field chamber (Accuscan Instruments). Open field chambers were cleaned thoroughly with Clidox prior to use. One mouse was placed in the center of each 40×40 cm open field chamber illuminated at 200 lux and left undisturbed for 20 min. Movement was tracked using the VersaMax software (Accuscan Instruments). Mice were removed from the open field chamber and each chamber was thoroughly cleaned with Clidox between experiments.

Social behavior

Social behavior was assessed in a 60×40 cm three-chamber apparatus with two clear plexiglass partitions. The apparatus was thoroughly disinfected with Clidox prior to use. A novel object (small orange cup) or a stranger mouse (wild-type mouse of the same sex and genetic background as the subject) were placed in containment cups in the left or right chambers. Subject mice were placed in the middle chamber with no access to other chambers for a 5 min acclimation period. Subjects were then allowed to freely move around the chambers for a period of

10 min. Following this, subjects were returned to the middle chamber with no access to the other chambers. The stranger mouse was moved with its containment cup to the opposite chamber. A novel stranger mouse was inserted in a clean containment cup in the chamber where the original stranger mouse was located. Access to all chambers was restored and subjects could explore freely for another 10 min. Movement was recorded using Ethovision XT, which generated tracking coordinates for each subject, analyzed as time spent within each chamber with a custom script. The three-chamber apparatus was thoroughly disinfected with Clidox between each subject.

Plethysmography

Respiration was monitored using a Buxco Whole Body Plethysmography (WBP) apparatus (Data Sciences International) according to manufacturer's instructions. All testing was conducted between the hours of 9 a.m. and 12 p.m. Mice were placed in plethysmography chambers and allowed to acclimate for 30 min, until motionless. Baseline breathing rates were measured for a period of 5 min. Breathing frequency, tidal volume and enhanced pause (PenH) were analyzed using Buxco FinePoint Software. Apneas were defined as cessation of breathing for over 1 s (two respiratory cycles) and were assessed manually over a period of baseline breathing.

Single-cell isolation and flow cytometry

P18 mouse lungs were collected from +/Y and *Mecp2*/Y mice at 9 a.m. A single-cell suspension was made as published, with modifications (56). Briefly, lungs were excised and incubated in fresh Hank's balanced salt solution (HBSS) with 5 U/ml dispase, 0.1% collagenase I and 0.002% DNase I for 30 min at room temperature. The lung was then disintegrated using forceps in a 6 cm petri dish. The cell suspension was filtered through 100, 70 and 30 μm nylon cell strainers. Red blood cells were lysed using RBC lysis buffer (Miltenyi Biotec). Cells were pelleted and resuspended in 500 μl staining media [SM: HBSS, 2% fetal bovine serum (Wisent), 10 mM 4-(2-hydroxyethyl)-1-piperazineethanesulfonic acid (HEPES), pH 7.2]. Cells were counted using the TC10/TC20 cell counter (BioRad). Approximately 3 million cells per sample were stained with fluorochrome-conjugated antibodies from BD Biosciences for 30 min on ice in the dark. Antibodies used were as follows: CD45.2 (558702), CD31 (561814), CD326 (563478), I-A/I-E (553623) and Podoplanin (566390). Cells were sorted using a MoFlo Astrios (Beckman Coulter) cell sorter. AE2 cells were as follows: CD45.2 $^{-}$, CD31 $^{-}$, CD326 $^{+}$, I-A/I-E $^{+}$, Podoplanin $^{-}$. Following sorting, cells were pelleted and re-suspended in fresh SM.

Single-cell RNA sequencing

For single-cell RNA sequencing, AE2 cells were isolated using flow cytometry from one +/Y and one *Mecp2*/Y mouse. Following cell sorting, over 95% of cells were negative for trypan blue (Invitrogen). Drop-seq was carried out at the Princess Margaret Genomics Facility (Toronto, Ontario) as previously described (57), using 2000 cells from each sample. Flow rates of 3000 $\mu\text{l}/\text{h}$ (cells and beads) and 13 000 $\mu\text{l}/\text{h}$ (oil) were used. Following Drop-seq droplet collection, complementary DNA (cDNA) amplification and library preparation were carried out as described (57). Libraries were sequenced on an Illumina NextSeq 500. FASTQ sequencing reads were processed, aligned to the mouse genome (mm10) and converted to digital gene expression matrices using

STAR aligner (STAR v2.5.2b). The CELLRANGER (v3.0.2) pipeline was used to obtain two types of gene-barcode matrices: the first is an unfiltered gene-barcode matrix and the second is the filtered gene-barcode matrix. The matrices were loaded into R (v3.5.1) for the final graphical output of results and statistical analysis using SCATER (v1.2.0), CELLRANGERRKIT (v1.1.0), SCRAN (v1.2.2), RTSNE (v0.11), SC3 (v1.3.14), EDGER (v3.16.5), SEURAT (v2.2.0) and PCAMETHODS (v1.50.0). After cell quality control, 1559 +/Y cells and 1524 *Mecp2*/Y cells remained. Low-abundance genes were filtered out and the dataset was normalized as previously published (58). Clustering and differential expression analyses were performed using a K-nearest neighbor algorithm and binary classifiers.

RNA extraction and RT-qPCR

Isolated AE2 cells or whole-lung RNA was used for RT-qPCR analysis. For whole-lung RNA, a 5 mm stainless steel bead (Qiagen, 69989) was added to chilled tubes containing lung tissue, which was then homogenized in 400 μ l of Qiazol using a Qiagen TissueLyser II. RNA extraction was carried out using the RNeasy Lipid Tissue Mini Kit (Qiagen, CA, USA) and stored at -80°C .

Reverse transcription of RNA was performed using the Superscript VILO cDNA synthesis kit (Invitrogen, CA, USA). Gene primers for RT-qPCR were designed to span exon-exon junctions of the gene of interest. RT-qPCR was performed using Power SYBR Green PCR Master Mix (Invitrogen) and the Viia7 instrument (ABI). PCR conditions were 95°C for 10 min, followed by 40 cycles of 95°C for 10 s and 60°C for 60 s. Single product amplification was confirmed by disassociation curves. Each sample was amplified three times for precision. The average cycle threshold (Ct) of these technical replicates was used to calculate expression. Gene expression was normalized to TATA-binding protein (*Tbp*) internal loading control and analyzed using the $2^{-\Delta\Delta\text{CT}}$ method. The primers used are included in [Supplementary Material, Table S2](#).

Protein extraction and western blotting

Mouse lungs were transferred to round bottom tubes with a 5 mm stainless steel bead (Qiagen, 69989) and 300 μ l of radioimmunoprecipitation assay buffer (RIPA) buffer [150 mM NaCl, 1% NP-40, 0.5% sodium deoxychlorate, 0.1% sodium dodecyl sulfate (SDS), 50 mM Tris, pH 8.0 and fresh protease inhibitors (Sigma-Aldrich, 11873580001)]. Tissues were lysed in a TissueLyser II (Qiagen, 85300) at 50 Hz for 2–3 min. Protein concentration was determined using a Bradford assay (Thermo Fisher, 23200). Proteins were separated in a 4–15% gradient sodium dodecyl sulfate-polyacrylamide gel electrophoresis (SDS-PAGE) gel (BioRad, 4561084). Proteins were transferred to a polyvinylidene fluoride (PVDF) membrane using the Trans-Blot SD semi-dry transfer cell (BioRad). Following transfer, membranes were blocked in 5% milk-Tris-buffered saline, 0.1% Tween 20. The following antibodies were used: anti-SREBP1 (Santa Cruz Biotechnology, sc-366; 1:500), anti-SREBP2 (abcam, ab30682; 1:500), anti-glyceraldehyde-3-phosphate dehydrogenase (GAPDH) (Cell Signaling, 5174, 1:2000), peroxidase-Affinipure goat anti-rabbit IgG (Jackson ImmunoResearch, 111-035-144). Proteins were visualized using Clarity western ECL (BioRad, 170-5060) and imaged on a Chemi-Doc (BioRad).

Nuclear protein extraction and immunoprecipitation

Nuclear extraction was performed as published (23). Briefly, frozen tissue was dounced with 1 ml of NE1 buffer (20 mM HEPES

pH 7.9, 10 mM KCl, 1 mM MgCl₂, 0.1% Triton X-100, 20% glycerol, protease inhibitor). Cells were pelleted and washed twice with NE1. Cells were then resuspended in 500 μ l of NE1 with 10 μ l of benzonase (Millipore 70746-3). Pellet was gently shaken at room temperature for 15 min. An equal volume of NE300 buffer (NE1 buffer with 5 mM NaCl) was added to the tubes and gently rotated for 30 min at 4°C . Tubes were spun at 16 000 g for 20 min at 4°C . Nuclear lysates (supernatant) were transferred to new tubes.

Immunoprecipitation was performed using the Millipore Catch and Release Kit (Millipore). Following manufacturer's instructions, 500 μ g of nuclear lysate was incubated with an anti-TBLR antibody (Bethyl Laboratories, A300-408A) for 3 h at 4°C . Following elution, half of the immunoprecipitated sample was loaded into each lane of a 4–20% gradient SDS-PAGE gel. Following transfer to a PVDF membrane, the following antibodies were used for western blotting: anti-MEC2P2 (Sigma-Aldrich, M7443), anti-HDAC3 (abcam, ab7030) and anti-NCOR1 (Bethyl Laboratories, A301-145A). Input samples represent 25 μ g of nuclear extracted protein.

ChIP

ChIP was performed as published (59). Briefly, frozen lungs were crosslinked by incubation in Solution A (1% formaldehyde, 50 mM HEPES-KOH, 100 mM NaCl, 1 mM ethylenediaminetetraacetic acid-EDTA, 0.5 mM ethylene glycol-bis(β -aminoethyl ether)-N,N,N',N'-tetraacetic acid-EGTA) for 20 min at room temperature, after which 2.5 M glycine was used to quench the reaction. Tissue was washed and dounced in ice-cold PBS with a loose and tight pestle. Dounced cells were filtered through a 100 μ m cell strainer and centrifuged. Protein G-Dynabeads (Invitrogen) were pre-blocked with 0.5% bovine serum albumin-BSA in PBS and bound to an anti-TBL1XR1 (TBLR1) antibody (Bethyl Laboratories, A300-408A) by overnight incubation at 4°C . Crosslinked cells were resuspended and washed in exchanges of LB1 (50 mM HEPES-KOH, 140 mM NaCl, 1 mM EDTA, 10% glycerol, 0.5% NP-40, 0.25% Triton X-100), LB2 (10 mM Tris-HCl, pH 8.0, 200 mM NaCl, 1 mM EDTA, 0.5 mM EGTA) and LB3 (10 mM Tris-HCl, pH 8.0, 100 mM NaCl, 1 mM EDTA, 0.5 mM EGTA, 0.1% Na-Deoxycholate, 0.5% N-lauroylsarcosine), each with fresh protease inhibitors. Chromatin in LB3 was transferred to 1.5 ml Bioruptor Pico microtubes (Diagenode C30010016) and sheared using the Bioruptor for nine cycles of 30 s on/30 s off (Diagenode). Sheared chromatin was incubated with beads overnight at 4°C . Beads were washed with ice-cold RIPA buffer (50 mM HEPES-KOH, pH 7.5, 500 mM LiCl, 1 mM EDTA, 1% Igepal CA-630, 0.7% Na-Deoxycholate) and TBS (20 mM Tris-HCl, pH 7.6, 150 mM NaCl). Chromatin was eluted from the beads in elution buffer (50 mM Tris-HCl, pH 8, 10 mM EDTA, 1% SDS) at 65°C overnight. Input and immunoprecipitated chromatin were treated with RNase A at 37°C for 30 min and Proteinase K at 55°C for 2 h. DNA was purified using SPRIME Phase Lock Gel Light tubes (QuantaBio) following the manufacturer's instructions. DNA pellets were washed with ethanol, dried and resuspended in 10 mM Tris-HCl, pH 8.0. Primers used for downstream qPCR analysis of immunoprecipitated and input DNA are listed in [Supplementary Material, Table S2](#).

Drug administration

As lipid metabolism follows a circadian rhythm, each treatment was administered at the same time of day, between 9 a.m. and 10 a.m. (ZT 2–3). Fluvastatin (Sellekchem) was dissolved

in 100% Dimethylsulfoxide-DMSO at 6 mg/ml. On the day of administration, aliquots of fluvastatin were diluted in sterile saline such that the desired dose for a 20 g mouse was given in 100 µl. Male mice were injected intraperitoneally with a twice weekly 1.5 mg/kg body weight dose from ages P28 to P56. Female mice were injected intraperitoneally with a weekly dose of 3 mg/kg body weight from 6 to 32 weeks of age. Vehicle controls (1:10 DMSO:saline) were administered at the same rate.

Statistics

The significance of the differences in mean values across two groups was evaluated by two-tailed Student t-tests. The statistical difference between four groups was evaluated using one-way or two-way analysis of variance with the Tukey post hoc test for multiple comparisons. Survival was assessed using the Logrank (Mantel-Cox) test. All statistical analyses were performed in GraphPad Prism (Version 7). P-values <0.05 were considered statistically significant.

Supplementary Material

Supplementary Material is available at HMG online.

Acknowledgements

The authors would like to thank Julie Ruston and Christine Taylor for technical assistance; Pradip Saha at the Mouse Metabolic and Phenotyping Core, Baylor College of Medicine, Houston, TX, and Denis Reynaud of The Analytical Facility for Bioactive Molecules, The Hospital for Sick Children, Toronto, Canada, for assistance with lipid quantification; and The Centre for Phenogenomics for assistance in mouse model production. The authors also thank Dr Lucy Osborne for thoughtful discussions and Dr Rebekah Tillotson, Julie Ruston, Laura Hergott and Steven Erwood for critical review.

Conflict of Interest statement. None declared.

Funding

The Angel Ava Fund (to M.J.J.); the Hospital for Sick Children Research Training Competition Award (RESTRACOMP) (to N.V.); the Canadian Institute of Health Research (GSD-157899 to N.V. and FDN-154273 to M.J.J.).

References

- Han, S.H. and Mallampalli, R.K. (2015) The role of surfactant in lung disease and host defense against pulmonary infections. *Ann. Am. Thorac. Soc.*, **12**, 765–774.
- Veldhuizen, E.J.A. and Haagsman, H.P. (2000) Role of pulmonary surfactant components in surface film formation and dynamics. *Biochim. Biophys. Acta Biomembr.*, **1467**, 255–270.
- Whitsett, J.A., Wert, S.E. and Weaver, T.E. (2010) Alveolar surfactant homeostasis and the pathogenesis of pulmonary disease. *Annu. Rev. Med.*, **61**, 105–119.
- Tredano, M., Griese, M., de Blic, J., Houdayer, C., Schumacher, S., Cartault, F., Capron, F., Boccon-Gibod, L., Lacaze-Masmonteil, T. and Renolleau, S. (2003) Analysis of 40 sporadic or familial neonatal and pediatric cases with severe

unexplained respiratory distress: relationship to SFTPB. *Am. J. Med. Genet.*, **119**, 324–339.

- Lawson, W.E., Cheng, D.S., Degryse, A.L., Tanjore, H., Polosukhin, V.V., Xu, X.C., Newcomb, D.C., Jones, B.R., Roldan, J., Lane, K.B. et al. (2011) Endoplasmic reticulum stress enhances fibrotic remodeling in the lungs. *Proc. Natl. Acad. Sci. U. S. A.*, **108**, 10562–10567.
- Ban, N., Matsumura, Y., Sakai, H., Takanezawa, Y., Sasaki, M., Arai, H. and Inagaki, N. (2007) ABCA3 as a lipid transporter in pulmonary surfactant biogenesis. *J. Biol. Chem.*, **282**, 9628–9634.
- Bridges, J.P., Schehr, A., Wang, Y., Huo, L., Besnard, V., Ikegami, M., Whitsett, J.A. and Xu, Y. (2014) Epithelial SCAP/INSIG/SREBP signaling regulates multiple biological processes during perinatal lung maturation. *PLoS One*, **9**, e91376.
- Lugaresi, E., Cirignotta, F. and Montagna, P. (1985) Abnormal breathing in the Rett syndrome. *Brain Dev.*, **7**, 329–333.
- Amir, R.E., Van den Veyver, I.B., Wan, M., Tran, C.Q., Francke, U. and Zoghbi, H.Y. (1999) Rett syndrome is caused by mutations in X-linked MECP2, encoding methyl-CpG-binding protein 2. *Nat. Genet.*, **23**, 185–188.
- Neul, J.L., Kaufmann, W.E., Glaze, D.G., Christodoulou, J., Clarke, A.J., Bahi-Buisson, N., Leonard, H., Bailey, M.E., Schanen, N.C., Zappella, M. et al. (2010) Rett syndrome: revised diagnostic criteria and nomenclature. *Ann. Neurol.*, **68**, 944–950.
- Anderson, A., Wong, K., Jacoby, P., Downs, J. and Leonard, H. (2014) Twenty years of surveillance in Rett syndrome: what does this tell us? *Orphanet J. Rare Dis.*, **9**, 1–9.
- Kerr, A.M. and Julu, P.O.O. (1999) Recent insights into hyperventilation from the study of Rett syndrome. *Arch. Dis. Child.*, **80**, 384–387.
- Saito, Y., Ito, M., Ozawa, Y., Matsuishi, T., Hamano, K. and Takashima, S. (2001) Reduced expression of neuropeptides can be related to respiratory disturbances in Rett syndrome. *Brain Dev.*, **23**, 122–126.
- Viemari, J.C., Roux, J.C., Tryba, A.K., Saywell, V., Burnet, H., Peña, F., Zanella, S., Bévençut, M., Barthelemy-Requin, M., Herzog, L.B. et al. (2005) Mecp2 deficiency disrupts norepinephrine and respiratory systems in mice. *J. Neurosci.*, **25**, 11521–11530.
- Weese-Mayer, D.E., Lieske, S.P., Boothby, C.M., Kenny, A.S., Bennett, H.L., Silvestri, J.M. and Ramirez, J.M. (2006) Autonomic nervous system dysregulation: breathing and heart rate perturbation during wakefulness in young girls with Rett syndrome. *Pediatr. Res.*, **60**, 443–449.
- Johnson, R.A., Lam, M., Punzo, A.M., Li, H., Lin, B.R., Ye, K., Mitchell, G.S. and Chang, Q. (2012) 7,8-dihydroxyflavone exhibits therapeutic efficacy in a mouse model of Rett syndrome. *J. Appl. Physiol.*, **112**, 704–710.
- Kron, M., Lang, M., Adams, I.T., Sceniak, M., Longo, F. and Katz, D.M. (2014) A BDNF loop-domain mimetic acutely reverses spontaneous apneas and respiratory abnormalities during behavioral arousal in a mouse model of Rett syndrome. *DMM Dis. Model. Mech.*, **7**, 1047–1055.
- Abdala, A.P., Dutschmann, M., Bissonnette, J.M. and Paton, J.F. (2010) Correction of respiratory disorders in a mouse model of Rett syndrome. *Proc. Natl. Acad. Sci.*, **107**, 18208–18213.
- Levitt, E.S., Hunnicutt, B.J., Knopp, S.J., Williams, J.T. and Bissonnette, J.M. (2013) A selective 5-HT_{1a} receptor agonist improves respiration in a mouse model of Rett syndrome. *J. Appl. Physiol.*, **115**, 1626–1633.

20. Szczesna, K., De La Caridad, O., Petazzi, P., Soler, M., Roa, L., Saez, M.A., Fourcade, S., Pujol, A., Artuch-Iriberry, R., Molero-Luis, M. et al. (2014) Improvement of the Rett syndrome phenotype in a *mecp2* mouse model upon treatment with levodopa and a DOPA-decarboxylase inhibitor. *Neuropsychopharmacology*, **39**, 2846–2856.
21. Voituron, N. and Hilaire, G. (2011) The benzodiazepine Midazolam mitigates the breathing defects of *Mecp2*-deficient mice. *Respir. Physiol. Neurobiol.*, **177**, 56–60.
22. Zhong, W., Johnson, C.M., Wu, Y., Cui, N., Xing, H., Zhang, S. and Jiang, C. (2016) Effects of early-life exposure to THIP on phenotype development in a mouse model of Rett syndrome. *J. Neurodev. Disord.*, **8**, 1–13.
23. Lyst, M.J., Ekiert, R., Ebert, D.H., Merusi, C., Nowak, J., Selfridge, J., Guy, J., Kastan, N.R., Robinson, N.D., de Lima Alves, F. et al. (2013) Rett syndrome mutations abolish the interaction of MeCP2 with the NCoR/SMRT co-repressor. *Nat. Neurosci.*, **16**, 898–902.
24. Tillotson, R., Selfridge, J., Koerner, M.V., Gadalla, K.K., Guy, J., De Sousa, D., Hector, R.D., Cobb, S.R. and Bird, A. (2017) Radically truncated MeCP2 rescues Rett syndrome-like neurological defects. *Nature*, **550**, 398–401.
25. Ebert, D.H., Gabel, H.W., Robinson, N.D., Kastan, N.R., Hu, L.S., Cohen, S., Navarro, A.J., Lyst, M.J., Ekiert, R., Bird, A.P. et al. (2013) Activity-dependent phosphorylation of MeCP2 threonine 308 regulates interaction with NCoR. *Nature*, **499**, 341–345.
26. Kruusvee, V., Lyst, M.J., Taylor, C., Tarnauskaitė, Ž., Bird, A.P. and Cook, A.G. (2017) Structure of the MeCP2–TBLR1 complex reveals a molecular basis for Rett syndrome and related disorders. *Proc. Natl. Acad. Sci.*, **114**, E3243–E3250.
27. Nott, A., Cheng, J., Gao, F., Lin, Y.T., Gjonneska, E., Ko, T., Minhas, P., Zamudio, A.V., Meng, J., Zhang, F. et al. (2016) Histone deacetylase 3 associates with MeCP2 to regulate FOXO and social behavior. *Nat. Neurosci.*, **19**, 1497–1505.
28. Mottis, A., Mouchiroud, L. and Auwerx, J. (2013) Emerging roles of the corepressors NCoR1 and SMRT in homeostasis. *Genes Dev.*, **27**, 819–835.
29. Feng, D., Liu, T., Sun, Z., Bugge, A., Mullican, S.E., Alenghat, T., Liu, X.S. and Lazar, M.A. (2011) A circadian rhythm orchestrated by histone deacetylase 3 controls hepatic lipid metabolism. *Science*, **331**, 1315–1319.
30. Kyle, S.M., Saha, P.K., Brown, H.M., Chan, L.C. and Justice, M.J. (2016) MeCP2 co-ordinates liver lipid metabolism with the NCoR1/HDAC3 corepressor complex. *Hum. Mol. Genet.*, **25**, 3029–3041.
31. Shahbazian, M.D., Antalffy, B., Armstrong, D.L. and Zoghbi, H.Y. (2002) Insight into Rett syndrome: MeCP2 levels display tissue- and cell-specific differences and correlate with neuronal maturation. *Hum. Mol. Genet.*, **11**, 115–124.
32. Uhlen, M., Oksvold, P., Fagerberg, L., Lundberg, E., Jonasson, K., Forsberg, M., Zwahlen, M., Kampf, C., Wester, K., Hober, S. et al. (2010) Towards a knowledge-based Human Protein Atlas. *Nat. Biotechnol.*, **28**, 1248–1250.
33. Buchovecky, C.M., Turley, S.D., Brown, H.M., Kyle, S.M., McDonald, J.G., Liu, B., Pieper, A.A., Huang, W., Katz, D.M., Russell, D.W. et al. (2013) A suppressor screen in *Mecp2* mutant mice implicates cholesterol metabolism in Rett syndrome. *Nat. Genet.*, **45**, 1013–1020.
34. Kida, H., Takahashi, T., Nakamura, Y., Kinoshita, T., Hara, M., Okamoto, M., Okayama, S., Nakamura, K., Kosai, K.I., Taniwaki, T. et al. (2017) Pathogenesis of lethal aspiration pneumonia in *Mecp2*-null mouse model for Rett syndrome. *Sci. Rep.*, **7**, 1–13.
35. Kriaucionis, S., Paterson, A., Curtis, J., Guy, J., MacLeod, N. and Bird, A. (2006) Gene expression analysis exposes mitochondrial abnormalities in a mouse model of Rett syndrome. *Mol. Cell. Biol.*, **26**, 5033–5042.
36. Pecorelli, A., Leoni, G., Cervellati, F., Canali, R., Signorini, C., Leoncini, S., Cortelazzo, A., De Felice, C., Ciccoli, L., Hayek, J. et al. (2013) Genes related to mitochondrial functions, protein degradation, and chromatin folding are differentially expressed in lymphomonocytes of Rett syndrome patients. *Mediat. Inflamm.*, **2013**, 1–18.
37. Shulyakova, N., Andrezza, A.C., Mills, L.R. and Eubanks, J.H. (2017) Mitochondrial dysfunction in the pathogenesis of Rett syndrome: implications for mitochondria-targeted therapies. *Front. Cell. Neurosci.*, **11**, 58.
38. Goldstein, J.L., DeBose-Boyd, R.A. and Brown, M.S. (2006) Protein sensors for membrane sterols. *Cell*, **124**, 35–46.
39. Horton, J.D., Goldstein, J.L. and Brown, M.S. (2002) SREBPs: activators of the complete program of cholesterol and fatty acid synthesis in the liver. *J. Clin. Invest.*, **109**, 1125–1131.
40. Hua, X., Yokoyama, C., Wu, J., Briggs, M.R., Brown, M.S., Goldstein, J.L. and Wang, X. (1993) SREBP-2, a second basic-helix-loop-helix-leucine zipper protein that stimulates transcription by binding to a sterol regulatory element. *Proc. Natl. Acad. Sci. U. S. A.*, **90**, 11603–11607.
41. Bertolio, R., Napoletano, F., Mano, M., Maurer-Stroh, S., Fantuz, M., Zannini, A., Biccato, S., Sorrentino, G. and Del Sal, G. (2019) Sterol regulatory element binding protein 1 couples mechanical cues and lipid metabolism. *Nat. Commun.*, **10**, 1–11.
42. LeBlanc, S.E., Srinivasan, R., Ferri, C., Mager, G.M., Gillian-Daniel, A.L., Wrabetz, L. and Svaren, J. (2005) Regulation of cholesterol/lipid biosynthetic genes by *Egr2/Krox20* during peripheral nerve myelination. *J. Neurochem.*, **93**, 737–748.
43. Kim, Y.M., Shin, H.T., Seo, Y.H., Byun, H.O., Yoon, S.H., Lee, I.K., Hyun, D.H., Chung, H.Y. and Yoon, G. (2010) Sterol regulatory element-binding protein (SREBP)-1-mediated lipogenesis is involved in cell senescence. *J. Biol. Chem.*, **285**, 29069–29077.
44. Kröner, C., Wittmann, T., Reu, S., Teusch, V., Klemme, M., Rauch, D., Hengst, M., Kappler, M., Cobanoglu, N., Sismanlar, T. et al. (2017) Lung disease caused by ABCA3 mutations. *Thorax*, **72**, 213–220.
45. Abildayeva, K., Jansen, P.J., Hirsch-Reinshagen, V., Bloks, V.W., Bakker, A.H., Ramaekers, F.C., De Vente, J., Groen, A.K., Wellington, C.L., Kuipers, F. et al. (2006) 24(S)-hydroxycholesterol participates in a liver X receptor-controlled pathway in astrocytes that regulates apolipoprotein E-mediated cholesterol efflux. *J. Biol. Chem.*, **281**, 12799–12808.
46. Villani, C., Sacchetti, G., Bagnati, R., Passoni, A., Fusco, F., Carli, M. and Invernizzi, R.W. (2016) Lovastatin fails to improve motor performance and survival in methyl-CpG-binding protein2-null mice. *elife*, **5**, e22409.
47. Justice, M.J., Buchovecky, C.M., Kyle, S.M. and Djukic, A. (2013) A role for metabolism in Rett syndrome pathogenesis: new clinical findings and potential treatment targets. *Rare Dis.*, **1**, e27265.
48. Segatto, M., Trapani, L., Di Tunno, I., Sticozzi, C., Valacchi, G., Hayek, J. and Pallottini, V. (2014) Cholesterol metabolism is altered in Rett syndrome: a study on plasma and primary cultured fibroblasts derived from patients. *PLoS One*, **9**, e104834.

49. Agudelo, C.W., Samaha, G. and Garcia-Arcos, I. (2020) Alveolar lipids in pulmonary disease. A review. *Lipids Health Dis.*, **19**, 1–21.
50. De Felice, C., Guazzi, G., Rossi, M., Ciccoli, L., Signorini, C., Leoncini, S., Tonni, G., Latini, G., Valacchi, G. and Hayek, J. (2010) Unrecognized lung disease in classic Rett syndrome: a physiologic and high-resolution CT imaging study. *Chest*, **138**, 386–392.
51. Ross, P.D., Guy, J., Selfridge, J., Kamal, B., Bahey, N., Tanner, K.E., Gillingwater, T.H., Jones, R.A., Loughrey, C.M., McCarrroll, C.S. et al. (2016) Exclusive expression of MeCP2 in the nervous system distinguishes between brain and peripheral Rett syndrome-like phenotypes. *Hum. Mol. Genet.*, **25**, 4389–4404.
52. Tarquinio, D.C., Hou, W., Neul, J.L., Berkmen, G.K., Drummond, J., Aronoff, E., Harris, J., Lane, J.B., Kaufmann, W.E., Motil, K.J. et al. (2018) The course of awake breathing disturbances across the lifespan in Rett syndrome. *Brain Dev.*, **40**, 515–529.
53. Remmerie, A. and Scott, C.L. (2018) Macrophages and lipid metabolism. *Cell. Immunol.*, **330**, 27–42.
54. Ryder, E., Doe, B., Gleeson, D., Houghton, R., Dalvi, P., Grau, E., Habib, B., Miklejewska, E., Newman, S., Sethi, D. et al. (2014) Rapid conversion of EUCOMM/KOMP-CSD alleles in mouse embryos using a cell-permeable Cre recombinase. *Transgenic Res.*, **23**, 177–185.
55. Guy, J., Gan, J., Selfridge, J., Cobb, S. and Bird, A. (2007) Reversal of neurological defects in a mouse model of Rett syndrome. *Science*, **315**, 1143–1147.
56. Singer, B.D., Mock, J.R., D'Alessio, F.R., Aggarwal, N.R., Mandke, P., Johnston, L. and Damarla, M. (2016) Flow-cytometric method for simultaneous analysis of mouse lung epithelial, endothelial, and hematopoietic lineage cells. *Am. J. Physiol. Lung Cell. Mol. Physiol.*, **310**, L796–L801.
57. Macosko, E.Z., Basu, A., Satija, R., Nemes, J., Shekhar, K., Goldman, M., Tirosh, I., Bialas, A.R., Kamitaki, N., Martersteck, E.M. et al. (2015) Highly parallel genome-wide expression profiling of individual cells using nanoliter droplets. *Cell*, **161**, 1202–1214.
58. Lun, A.T.L., Bach, K. and Marioni, J.C. (2016) Pooling across cells to normalize single-cell RNA sequencing data with many zero counts. *Genome Biol.*, **17**, 1–14.
59. Schmidt, D., Wilson, M.D., Spyrou, C., Brown, G.D., Hadfield, J. and Odom, D.T. (2009) ChIP-seq: using high-throughput sequencing to discover protein-DNA interactions. *Methods*, **48**, 240–248.